Cavity-Enhanced Optical Readout of a Single Solid-State Spin

Shuo Sun,[1] Hyochul Kim,[1] Glenn S. Solomon,[2] and Edo Waks[1,*]

[1]*Department of Electrical and Computer Engineering, Institute for Research in Electronics and Applied Physics, and Joint Quantum Institute, University of Maryland, College Park, Maryland 20742, USA*

[2]*Joint Quantum Institute, University of Maryland and National Institute of Standards and Technology, College Park, Maryland 20742, USA*

(Received 17 June 2017; revised manuscript received 4 April 2018; published 9 May 2018)

We demonstrate optical readout of a single spin using cavity quantum electrodynamics. The spin is based on a single trapped electron in a quantum dot that has a poor branching ratio of 0.43. Selectively coupling one of the optical transitions of the quantum dot to the cavity mode results in a spin-dependent cavity reflectivity that enables spin readout by monitoring the reflected intensity of an incident optical field. Using this approach, we demonstrate spin-readout fidelity of 0.61. Achieving this fidelity using resonance fluorescence from a bare dot would require 43 times improvement in photon collection efficiency.

DOI: 10.1103/PhysRevApplied.9.054013

I. INTRODUCTION

Spins in solids are promising qubit systems for quantum information applications due to their scalability and prospects for developing compact chip-integrated devices [1,2]. Scalable quantum technology requires methods to measure these spins with high speed and fidelity [3]. Optical spin readout provides one of the fastest and most precise measurement methods [4,5], and is thus highly desirable for scalable quantum information processing.

Optical readout approaches typically rely on resonance fluorescence [6–10], resonance absorption [11], or optical Kerr or Faraday rotations [12–14]. The readout fidelity of these approaches is limited by the branching ratio of the spin system, defined as the probability that an optical excitation induces a spin flip due to an undesired decay channel [15]. For example, for resonance fluorescence spectroscopy, the branching ratio determines the number of photons generated by the cycling transition before the measurement induces a spin flip. Many confined spin systems such as quantum dot spins [16], fluorine impurities [17], and silicon-vacancy centers in diamond [18,19] do not possess a good branching ratio due to nonradiative decay mechanisms or poor selection rules. In addition, the external magnetic field direction to achieve the optimal branching ratio for these confined spin systems typically conflicts with the condition that allows coherent optical spin manipulations [20–23]. These qubit systems therefore require alternative methods for readout.

Optical cavities can significantly improve qubit readout. For example, cavities can enable quantum nondemolition measurements of the hyperfine states of single atoms by probing absorption without scattering the atom out of the trap [24–26], thereby preserving its quantum state. In solid-state systems, planar distributed Bragg reflector cavities showed impressive spin-readout fidelity at the single-shot level [10]. The cavity utilized in this work serves to facilitate the extraction of photons from the substrate, but does not exhibit strong light-matter coupling in the form of a Purcell effect due to a low cavity quality factor and high mode volumes. More recent theoretical work showed that cavities operating in the high-cooperativity regime where light-matter interactions are strong can enable high-fidelity spin readout [27–29], even when the qubit has a poor branching ratio [30]. In this approach, the cavity directly modifies the radiative properties of the spin transition, while the emitter induces a spin-dependent reflectance or transmittance of a cavity that efficiently couples to an external readout laser [31–33]. This strong coupling of light to matter fundamentally improves the readout fidelity beyond the limits imposed by the branching ratios of the bare system, enabling high-fidelity spin readout in a broad range of physical systems lacking appropriate cycling transitions. However, such a cavity-enhanced spin readout remains to be experimentally demonstrated.

In this paper, we demonstrate enhanced optical readout of a single solid-state spin using cavity quantum electrodynamics. We demonstrate this spin-readout approach using a spin contained in a single InAs quantum dot coupled to a photonic crystal cavity. Selectively coupling one of the optical transitions of the quantum dot to the cavity mode results in a spin-dependent cavity reflectivity that enables spin readout by monitoring the reflected intensity of an incident optical field. Using this approach, we demonstrate spin-readout fidelity of 0.61. Achieving

*edowaks@umd.edu

 © 2018 American Physical Society

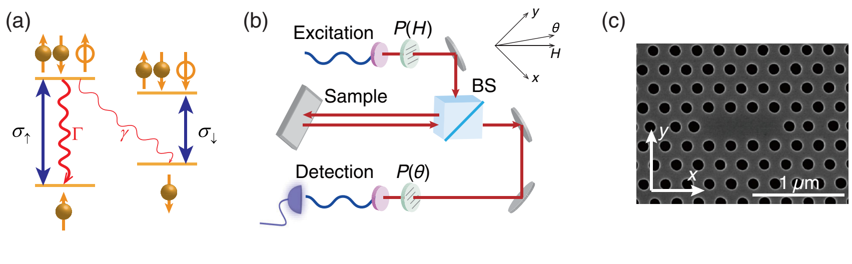

FIG. 1. (a) Energy level structure of a charged quantum dot in the presence of a magnetic field applied in the Faraday geometry. (b) Schematic setup for optical spin readout based on cavity quantum electrodynamics. BS, beam splitter; $P(H)$, polarizer along H direction; $P(\theta)$, polarizer along the θ direction. (c) Scanning electron microscope image of a fabricated photonic crystal cavity device.

this fidelity using resonance fluorescence from a bare dot would require 43 times improvement in photon collection efficiency.

II. PROTOCOL FOR CAVITY-ENHANCED SPIN READOUT

Figure 1(a) shows the level structure of the charged quantum dot, which is composed of two ground states corresponding to spin states of the electron, denoted $|\uparrow\rangle$ and $|\downarrow\rangle$, and two excited trion states composed of two electrons and a hole, which we denote as $|\Uparrow\rangle$ and $|\Downarrow\rangle$ to highlight the spin of the hole. The spin-conserving transitions $|\Uparrow\rangle \rightarrow |\uparrow\rangle$ and $|\Downarrow\rangle \rightarrow |\downarrow\rangle$ are optically allowed, denoted as $\sigma_\uparrow$ and $\sigma_\downarrow$ in the figure. The cross transitions $|\Uparrow\rangle \rightarrow |\downarrow\rangle$ and $|\Downarrow\rangle \rightarrow |\uparrow\rangle$ are forbidden for excitons composed purely of heavy holes, but heavy-hole light-hole mixing will render these transitions partially allowed [34]. A magnetic field applied along the growth direction (Faraday geometry) breaks the degeneracy of the optical transitions, but does not significantly alter the selection rules [16]. We define the branching ratio of a quantum dot as $R_B = \gamma/(\Gamma + \gamma)$ [15], where Γ is the spontaneous emission rate of the optically allowed transition $|\Uparrow\rangle \rightarrow |\uparrow\rangle$ for a bare quantum dot, and γ is the decay rate of transition $|\Uparrow\rangle \rightarrow |\downarrow\rangle$.

We follow the spin-readout method described and analyzed in Ref. [30]. In our implementations, transition $\sigma_\uparrow$ resonantly couples with a single-sided optical cavity, whereas transition $\sigma_\downarrow$ is decoupled due to a large detuning induced by an external magnetic field. For a single incident photon that is resonant with the cavity, the cavity reflection coefficients in the cases of spin-up and spin-down states are given by $r_\uparrow = 1 - [2\alpha/(C+1)]$ and $r_\downarrow = 1 - 2\alpha$, respectively [31–33], where $C = 2g^2/\kappa\Gamma_d$ is the atomic cooperativity and $\alpha = \kappa_{ex}/\kappa$ is the interference contrast. In these expressions, g is the coupling strength between transition $\sigma_\uparrow$ and the cavity mode, κ is the energy decay rate of the cavity, $\Gamma_d = [(\Gamma + \gamma)/2] + \gamma_d$ is the dipole decay rate of transition $\sigma_\uparrow$ where γ_d is the dipole decoherence rate, κ_{ex} is the cavity energy decay rate to the reflected mode. In the ideal limit of high interference contrast ($\alpha = 1$) and high cooperativity ($C \gg 1$), the reflection coefficients become $r_\uparrow = 1$ and $r_\downarrow = -1$. Thus, a photon picks up a spin-dependent π phase shift upon reflection, which distinguishes the two spin states. Nonideal cooperativity and interference contrast will degrade the amplitudes of the coefficients but will still lead to a change of phase shift provided $\alpha > 0.5$ and $C > 1$.

In order to convert the spin-dependent phase shift to an optical signal that performs readout, we use the polarization interferometry setup illustrated in Fig. 1(b). We inject a weak coherent field whose polarization is oriented at a 45° angle relative to the cavity polarization axis. The polarization component that is along the cavity is reflected with a spin-dependent phase shift, whereas the orthogonal polarization component is directly reflected from the sample surface with no phase shift. We send the reflected field to a polarizer rotated at an angle θ relative to the cavity polarization axis and focus it onto a single-mode fiber. A single-photon detector monitors the field intensity to perform spin readout. In the Supplemental Material, Sec. 1 [35], we show that by properly selecting the angle θ, we attain a collection probability of $P = (1/4)\beta|1 + r_{\uparrow,\downarrow}|^2$ for a cavity-coupled incident photon, where β is the coupling efficiency from the cavity spatial mode to the collection fiber. Therefore, the detector will not detect any photons when the spin is in the spin-down state ($r_\downarrow = -1$), but will detect a bright photon flux for spin-up state ($r_\uparrow = 1$). The system implements a spin readout in an analogous way to resonance fluorescence spectroscopy.

The spin-readout fidelity is limited by the number of photons reflected into the detection polarization basis before a spin-flip event occurs. If we use resonance fluorescence from a bare dot to measure the spin, the maximum number of photons we can extract is $N' = (1 - R_B)/R_B$. The number of reflected photons using the cavity quantum electrodynamics approach is instead given by $N = (2g^2/\kappa\Gamma)N'$ (see Supplemental Material, Sec. 2 [35]). In photonic crystal cavities the enhancement factor $2g^2/\kappa\Gamma$ can be as high as 1300 [36], which could correspond to a 3 orders-of-magnitude improvement in the number of detected photons.

III. DEVICE DESIGN, FABRICATION, AND CHARACTERIZATION

We couple the quantum dot with a photonic crystal cavity. Figure 1(c) shows the scanning electron microscope image of the fabricated photonic crystal cavity. The initial wafer for device fabrication is composed of a 160-nm-thick GaAs membrane with a single layer of InAs quantum dots at its center (density of 10–50/μm^2). A fraction of quantum dots in the sample are naturally charged due to the residual doping background. We use a weak white-light illumination to stabilize the extra electron confined in the dot. The membrane layer is grown on top of a 900-nm-thick $Al_{0.78}Ga_{0.22}As$ sacrificial layer. A distributed Bragg reflector composed of 10 layers of GaAs and AlAs is grown below the sacrificial layer and acts as a high reflectivity mirror, creating a one-sided cavity. Photonic crystal structures are defined using electron-beam lithography, followed by inductively coupled plasma dry etching and selective wet etching of the sacrificial $Al_{0.78}Ga_{0.22}As$ layer. The cavity is composed of a three-hole defect in a triangular photonic crystal with a lattice constant of 240 nm and a hole radius of 72 nm, where we shift the inner three holes adjacent to the defect to optimize the quality factor [37]. The cavity supports a small mode volume of $0.7(\lambda/n)^3$ [38], where λ is the cavity resonant wavelength and n is the refractive index of the GaAs substrate.

To optically characterize the device, we mount the sample in a closed-cycle cryostat that cools the sample to 3.6 K. An integrated superconducting magnet system applies a magnetic field of up to 9.2 T in the out-of-plane (Faraday) configuration. We excite the sample and collect the reflected signal using a confocal microscope with an objective lens that has a numerical aperture of 0.82. A single-mode fiber spatially filters the collected signal to remove spurious surface reflection. We perform spectral measurements using a grating spectrometer with a spectral resolution of 7 GHz. To measure the temporal properties of the signal we perform photon counting measurements using a single-photon counting module (SPCM-NIR-14) with a time resolution of 800 ps.

We estimate an overall photon detection efficiency of our system to be 0.41%, which includes the collection efficiency of the objective lens (4.5%), transmission efficiency for a 90/10 beam splitter (90%), a fiber connector (73%), and a fiber Fabry-Perot tunable filter (40%), and the quantum efficiency of the detector (35%).

We first characterize the device by performing reflectivity measurements using a broadband LED [39]. We set the detection polarization to be orthogonal to the input field. Figure 2(a) shows the reflection spectrum as a function of magnetic field. At 0 T, the spectrum shows a bright peak due to the cavity (labeled as CM) and a second peak due to the quantum dot (labeled as QD), which is red detuned from the cavity resonance by 0.27 nm (94 GHz). At a higher magnetic field the quantum dot splits into two peaks, corresponding to the $\sigma_\uparrow$ and $\sigma_\downarrow$ transitions shown in Fig. 1(a). Measurements with a magnetic field applied in the Voigt configuration verify that the quantum dot is charged (see Supplemental Material, Sec. 3. 1 [35]).

To set the polarization analyzer to the optimal orientation for spin readout, we set the magnetic field to 0 T so that the dot is highly detuned from the cavity. We then orient the polarization analyzer to minimize the measured field intensity at the cavity resonance, which results in the cavity spectrum shown as red diamonds in Fig. 2(b). We obtain this spectrum by scanning the frequency of a tunable narrow bandwidth (<300 kHz) laser and monitor its reflected intensity at each frequency. We then increase the magnetic field to 3.7 T, where transition $\sigma_\uparrow$ is resonant with the cavity mode. We also introduce a second narrow bandwidth laser resonant with the $\sigma_\downarrow$ transition to optically pump the spin to the spin-up state [40]. The blue circles in Fig. 2(b) show the resulting spectrum. The cavity spectrum now exhibits a peak at the cavity resonance, resulting in 16 times enhancement of the cavity reflected intensity compared with the bare cavity spectrum.

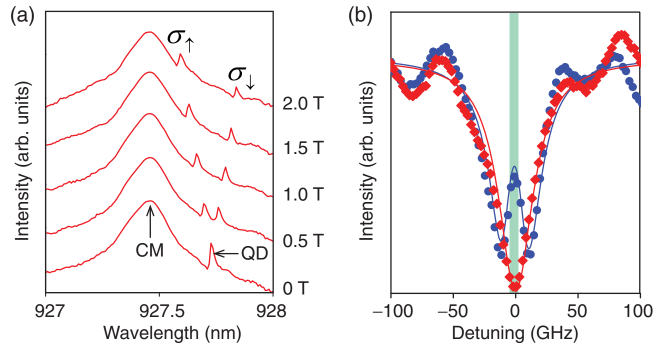

FIG. 2. (a) Cross-polarized reflectivity of the device at several different magnetic fields. (b) Cavity reflectivity at a magnetic field of 0 T (red diamonds) and 3.7 T (blue circles). Blue and red solid lines show the calculated spectra.

The solid lines in Fig. 2(b) are the calculated reflection spectra which we attain from a numerical fit to a master equation that accounts for dissipation and dephasing. We provided the details of these calculations in a previous work [41]. From the numerical fit we can extract all the parameters of the system: $g/2\pi = 10.2 \pm 0.1$ GHz, $\kappa/2\pi = 33.5 \pm 0.6$ GHz, $\Gamma_d/2\pi = 4.2 \pm 0.2$ GHz, and $\alpha = 0.92 \pm 0.01$. Using these values, we obtain a cooperativity of $C = 1.46 \pm 0.08$. We also estimate the enhancement factor to be $N/N' = 62$ using the previously reported value of $\Gamma/2\pi = 0.1$ GHz for a bulk quantum dot [42]. The coupling strength satisfies the condition $g > \kappa/4$, indicating that we are operating at the onset of the strong coupling regime.

IV. MEASUREMENT OF CAVITY-ENHANCED SPIN READOUT

To perform spin readout, we use a pump-probe pulse sequence shown in Fig. 3(a), which measures the time evolution of the cavity reflection. We generate the pump and probe pulses out of two narrow bandwidth continuous-wave lasers, each of which is modulated by an electro-optic modulator. The pump pulse prepares the spin to either the spin-up or spin-down state by resonantly pumping either

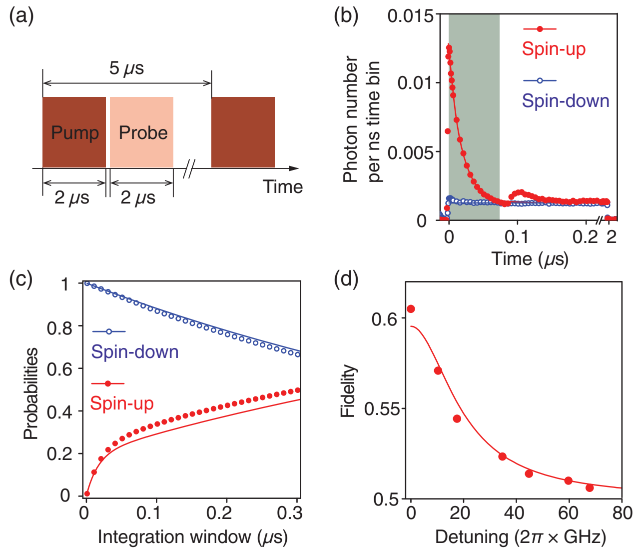

FIG. 3. (a) Pump-probe pulse sequence for spin-readout measurements. (b) Intensity of the reflected probe pulse. The blue open circles and the red filled circles show the measured data when the spin is initialized in the spin-down and spin-up state, respectively. The blue and red solid lines show a numerical fit to a constant and an exponential function, respectively. (c) Detection probability of spin-up state (red) and spin-down state (blue) as a function of the integration window length. The blue open circles and red filled circles show the measured probability, and the blue and red solid lines show the numerical calculated probability. (d) Fidelity as a function of detuning between transition $\sigma_\uparrow$ and the cavity. Red circles show measured value at several detuning conditions, and the red solid line shows a numerical fit.

the $\sigma_\downarrow$ or $\sigma_\uparrow$ transition. The probe pulse is always resonant with the cavity. We set the peak power of the pump pulse to be 710 nW, which is well beyond the saturation power for both transition $\sigma_\downarrow$ and $\sigma_\uparrow$. We set the peak power of the probe pulse to be 50 nW (measured before the objective lens), corresponding to 0.14 photons per modified lifetime of transition $\sigma_\uparrow$ (see Supplemental Material, Sec. 3.2 [35] for characterization of in-coupling efficiency from the objective lens to the cavity which is determined to be 4.5%). This probe power achieves the optimal spin-readout performance (see Supplemental Material, Sec. 4 [35] for power-dependent spin-readout measurement), because it is small enough to satisfy the weak excitation regime, but sufficiently large so that the spin-flip rate of the dot is dominated by photon backaction rather than the intrinsic spin decay (see Supplemental Material, Sec. 3.3 [35] for intrinsic spin-flip time measurement). We set the duration of both pump and probe pulses to be 2 μs, which is long enough compared with the spin-flip time induced by both the pump (<6 ns) and probe fields (17.6 ns).

Figure 3(b) shows the intensity of the reflected probe pulse when we initialize the spin to the spin-up (red filled circles) and spin-down (blue open circles) states, respectively. Initially, the reflected intensity for the spin-up case is 9 times higher than the spin-down case, but it decays over time due to optically induced spin flips. The red and blue solid lines show numerical fit of the measured data to an exponential function (for the spin-up state) and a constant background (for the spin-down state), respectively. The intensity for the spin-up case exponentially decays with a time constant of 17.6 ns because the probe laser induces a spin flip. The signal decays to a finite background level which is caused by the imperfect extinction of the cavity signal and an imperfect spin initialization fidelity of 0.95. We attribute the second bump around 100 ns, which is also present when we directly inject the laser onto the detectors, to the after pulse of the photon detector. The dark counts of the detector are more than 3 orders of magnitude lower than the reflected intensity at the spin-down case, and therefore constitute a negligible contribution to the overall signal.

The choice of integration time plays a crucial role in the spin-readout scheme. Longer integration times result in a larger number of collected photons. However, as shown in Fig. 3(b), after 80 ns the spin-up state decays to the spin-down state due to optically induced spin flips. Integrating beyond this time window will only add background photons without increasing the signal.

We define $P_\uparrow$ as the probability of detecting at least one photon reflected from the cavity when the dot is initially in the spin-up state, and $P_\downarrow$ as the probability of detecting zero photons when the spin is initially in the spin-down state. Figure 3(c) plots the measured $P_\uparrow$ (red filled circles) and $P_\downarrow$ (blue open circles) as a function of the integration time. To measure these values, we repeat the pulse sequence shown in Fig. 3(a) for $n = 2\,000\,000$ times, and calculate the probabilities as $P_\uparrow = n_\uparrow/n$ and $P_\downarrow = 1 - n_\downarrow/n$, where $n_\uparrow$ and $n_\downarrow$ are the number of measurements that register at least a photon within an integration time window for the spin-up and spin-down initialization, respectively. The red and blue solid lines show numerically calculated values for $P_\uparrow$ and $P_\downarrow$ based on the average photon number detected within each integration window obtained in Fig. 3(b). These calculations assume Poisson counting statistics for the detected photons. The small deviation between the experiment and calculation is due to detector dead time, which results in experimental counting statistics that slightly deviate from a Poisson distribution.

The probability $P_\uparrow$ initially increases rapidly as we collect more signal, but tapers off after approximately 80 ns due to collected background photons. In contrast, $P_\downarrow$ continually decreases as we increase the integration window due to background photons. From these two probabilities, we can calculate the spin-readout fidelity given by $F = (P_\uparrow + P_\downarrow)/2$ [10], which achieves an optimal value of $F = 0.61 \pm 0.0005$ at a window of 75 ns [indicated as the gray bar in Fig. 3(b)]. At this optimal window, we detect an average number of 0.3 photons for the spin-up state, and 0.1 photons for the spin-down state.

We note that because the optimal measurement time of 75 ns is longer than the laser-induced spin-flip time of 17.6 ns, the measurement destroys the quantum state of the spin.

Figure 3(d) shows the measured optimal spin-readout fidelity as a function of detuning Δ between transition $\sigma_\uparrow$ and the cavity. To control the detuning, we reduce the applied magnetic field, and adjust the probe center frequency to always be resonant with transition $\sigma_\uparrow$. We also optimize the detection polarization at each detuning by adding another rotatable quarter-wave plate, so that the reflected probe intensity is always maximally suppressed when the dot is in the spin-down state (see Supplemental Material, Sec. 5 [35]). The fidelity achieves the maximum at the resonance condition, and rapidly decays as we detune from the cavity resonance, demonstrating that the improved signal is due to cavity enhancement. The red solid line in Fig. 3(d) shows a numerical calculation of the fidelity as a function of detuning Δ assuming a linear photon detector (i.e., no dead time; see Supplemental Material, Sec. 6 [35]), which agrees well with the measured results.

V. DISCUSSIONS

It is instructive to compare the performance of the cavity readout approach to what we would attain using resonance fluorescence from the bare quantum dot (not coupled to the cavity). In a resonance fluorescence measurement, the average number of photons that the bare quantum dot could emit via the cycling transition is given by $N' = \Gamma/\gamma$, or equivalently, $N' = (1 - R_B)/R_B$, where R_B is the branching ratio. In the shot noise limit, the probability $P_\uparrow$ is given by $P_\uparrow = 1 - \exp(-\eta N')$, where η is the overall detection efficiency of emitted photons. In the absence of dark counts and background signal, the fidelity is given by $F' = [(1 + P_\uparrow)/2] = 1 - (1/2)e^{-\eta(1-R_B)/R_B}$. This expression puts a fundamental limit on the attainable fidelity using resonance fluorescence from the bare dot.

Figure 4(a) plots the expected fidelity of the system (red solid line) and the upper bound to the fidelity of the bare dot (blue dashed line) as a function of overall photon detection efficiency (see Supplemental Material, Sec. 6 [35] for a description of numerical calculation). The black square shows the experimentally measured value for using the cavity approach, which shows a spin-readout fidelity of 0.61 at an overall detection efficiency of $\eta = 0.41\%$. We attribute the slight mismatch between the experimental data point and the theoretical curve to uncertainty in the efficiency, which depends on the specific alignment condition. If we read out the spin based on the resonance fluorescence from a bare dot, at the same overall photon detection efficiency, we would obtain a fidelity of $F' = 0.503$, which is very close to a fidelity of 0.5 where the measurement provides no information about the spin state. Even with an overall photon detection efficiency of 1, the upper bound fidelity for using resonance fluorescence from a bare dot is only 0.87. This poor fidelity is due to the poor branching ratio of this dot of 0.43 (see Supplemental Material, Sec. 3.2 [35] for a measurement of the quantum dot branching ratio). To achieve a fidelity of $F = 0.61$ using resonance fluorescence of the bare dot would require an efficiency of 17.8%, which corresponds to 43 times improvement.

The shaded area is the region where the fidelity exceeds 0.82, which is conventionally defined as the single-shot measurement regime [10]. With the cavity quantum electrodynamics approach, single-shot readout requires an overall detection efficiency of 1.7%, which is only a factor of 4

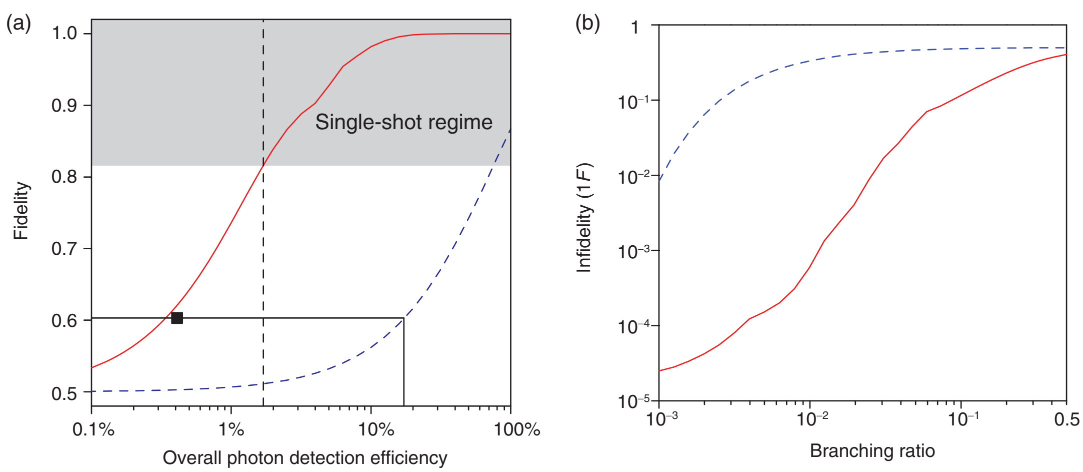

FIG. 4. (a) Expected fidelity of our system (red solid line) and the upper bound fidelity for bare dot resonance fluorescence (blue dashed line) as a function of overall photon detection efficiency. The black square shows the measured value for our current device. The vertical dashed line shows the efficiency to achieve the single-shot limit using our device. (b) Expected infidelity of our system (red solid line) and the lower bound infidelity for bare dot resonance fluorescence (blue dashed line) as a function of the quantum dot branching ratio.

larger than our current system efficiency. Thus, even for this dot that has a very poor branching ratio, our cavity approach is close to the single-shot regime.

We note that previous works reported a spin-readout fidelity of 0.82 using resonance fluorescence spectroscopy, which is within the single-shot limit [10]. These measurements achieved the single-shot regime because they used a quantum dot with a branching ratio of 0.002, which is more than 2 orders of magnitude better than the branching ratio of the dot used in this work. Figure 4(b) plots the expected infidelity $D = 1 - F$ of the cavity-enhanced readout approach (red solid line), along with the fundamental bound for the resonance fluorescence approach on a bare dot (blue dashed line) as a function of the quantum dot branching ratio. We assume an overall photon detection efficiency of 0.41% in the calculation, equal to the efficiency of our system. The results show that a branching ratio of 10^{-2} to 10^{-3}, which are attainable in charge-stabilized quantum dots [10,15], would enable a readout infidelity of 10^{-3} to 10^{-4}. These values are highly promising for efficient quantum error correction [43]. In contrast, bare resonance fluorescence can attain an infidelity of only 5×10^{-2}.

VI. CONCLUSIONS

In summary, we demonstrate optical readout of a single solid-state spin by using strong light-matter interactions with an optical cavity. We show that the cavity enables spin readout with a fidelity of 0.61 for a quantum dot that has a poor branching ratio of 0.43. To achieve the same value using resonance fluorescence requires a factor of 43 improvement in photon collection efficiency. Our current experiment is only a factor of 4 away in efficiency from the single-shot regime. We could potentially improve this efficiency by replacing our avalanche photodiode detectors with superconducting nanowire detectors that could provide a factor of 3 increase in detection efficiency. Our collection efficiency is also low (4.5%) due to the finite numerical aperture of the objective lens. Directional photonic crystal cavity designs [44] or micropost cavities [45,46] that provide a highly collimated transverse mode could significantly improve this efficiency. Directly extracting light to a waveguide could also increase the efficiency [47]. For quantum dot spin readout, charge-stabilized dots embedded in a diode membrane could significantly improve readout fidelity since they possess a much better branching ratio. Such diode structures can also be incorporated in photonic crystal cavities as demonstrated by recent works [48,49]. Because of the scalable nature of the photonic crystal platform, our results can be directly applied to integrated devices composed of waveguides and cavities that exhibit similar strong light-matter interactions [50]. Combining with recently developed technologies for on-chip photon detection [51,52], our results could eventually lead to chip-integrated solid-state qubit measurements, which paves the way towards quantum information processing with compact on-chip devices.

ACKNOWLEDGMENTS

The authors would like to acknowledge fruitful discussions with Dr. Edward Flagg. This work is supported by the DARPA QUINESS program (Grant No. W31P4Q1410003), the Physics Frontier Center at the Joint Quantum Institute, the National Science Foundation (Grant No. PHYS. 1415458), and the Center for Distributed Quantum Information.

[1] J. L. O'brien, A. Furusawa, and J. Vučković, Photonic quantum technologies, Nat. Photonics **3**, 687 (2009).

[2] D. D. Awschalom, L. C. Bassett, A. S. Dzurak, E. L. Hu, and J. R. Petta, Quantum spintronics: Engineering and manipulating atom-like spins in semiconductors, Science **339**, 1174 (2013).

[3] D. P. DiVincenzo, The physical implementation of quantum computation, Fortschr. Phys. **48**, 771 (2000).

[4] F. Jelezko and J. Wrachtrup, Read-out of single spins by optical spectroscopy, J. Phys. Condens. Matter **16**, R1089 (2004).

[5] W. Gao, A. Imamoglu, H. Bernien, and R. Hanson, Coherent manipulation, measurement and entanglement of individual solid-state spins using optical fields, Nat. Photonics **9**, 363 (2015).

[6] A. N. Vamivakas, Y. Zhao, C.-Y. Lu, and M. Atatüre, Spin-resolved quantum-dot resonance fluorescence, Nat. Phys. **5**, 198 (2009).

[7] P. Neumann, J. Beck, M. Steiner, F. Rempp, H. Fedder, P. R. Hemmer, J. Wrachtrup, and F. Jelezko, Single-shot readout of a single nuclear spin, Science **329**, 542 (2010).

[8] A. N. Vamivakas, C.-Y. Lu, C. Matthiesen, Y. Zhao, S. Fält, A. Badolato, and M. Atatüre, Observation of spin-dependent quantum jumps via quantum dot resonance fluorescence, Nature (London) **467**, 297 (2010).

[9] L. Robledo, L. Childress, H. Bernien, B. Hensen, P. F. Alkemade, and R. Hanson, High-fidelity projective read-out of a solid-state spin quantum register, Nature (London) **477**, 574 (2011).

[10] A. Delteil, W.-b. Gao, P. Fallahi, J. Miguel-Sanchez, and A. Imamoğlu, Observation of Quantum Jumps of a Single Quantum Dot Spin Using Submicrosecond Single-Shot Optical Readout, Phys. Rev. Lett. **112**, 116802 (2014).

[11] X. Xu, Y. Wu, B. Sun, Q. Huang, J. Cheng, D. Steel, A. Bracker, D. Gammon, C. Emary, and L. Sham, Fast Spin State Initialization in a Singly Charged InAs-GaAs Quantum Dot by Optical Cooling, Phys. Rev. Lett. **99**, 097401 (2007).

[12] J. Berezovsky, M. Mikkelsen, O. Gywat, N. Stoltz, L. Coldren, and D. Awschalom, Nondestructive optical measurements of a single electron spin in a quantum dot, Science **314**, 1916 (2006).

[13] M. Atatüre, J. Dreiser, A. Badolato, and A. Imamoglu, Observation of Faraday rotation from a single confined spin, Nat. Phys. **3**, 101 (2007).

[14] M. Mikkelsen, J. Berezovsky, N. Stoltz, L. Coldren, and D. Awschalom, Optically detected coherent spin dynamics of a single electron in a quantum dot, Nat. Phys. **3**, 770 (2007).

[15] C.-Y. Lu, Y. Zhao, A. Vamivakas, C. Matthiesen, S. Fält, A. Badolato, and M. Atatüre, Direct measurement of spin dynamics in InAs/GaAs quantum dots using time-resolved resonance fluorescence, Phys. Rev. B **81**, 035332 (2010).

[16] M. Bayer, G. Ortner, O. Stern, A. Kuther, A. Gorbunov, A. Forchel, P. Hawrylak, S. Fafard, K. Hinzer, and T. Reinecke, Fine structure of neutral and charged excitons in self-assembled In(Ga)As/(Al)GaAs quantum dots, Phys. Rev. B **65**, 195315 (2002).

[17] Y. Kim, D. Sleiter, K. Sanaka, Y. Yamamoto, J. Meijer, K. Lischka, and A. Pawlis, Semiconductor qubits based on fluorine implanted ZnMgSe/ZnSe quantum-well nanostructures, Phys. Rev. B **85**, 085302 (2012).

[18] L. J. Rogers, K. D. Jahnke, M. W. Doherty, A. Dietrich, L. P. McGuinness, C. Müller, T. Teraji, H. Sumiya, J. Isoya, and N. B. Manson, Electronic structure of the negatively charged silicon-vacancy center in diamond, Phys. Rev. B **89**, 235101 (2014).

[19] T. Müller, C. Hepp, B. Pingault, E. Neu, S. Gsell, M. Schreck, H. Sternschulte, D. Steinmüller-Nethl, C. Becher, and M. Atatüre, Optical signatures of silicon-vacancy spins in diamond, Nat. Commun. **5**, 3328 (2014).

[20] X. Xu, B. Sun, P. R. Berman, D. G. Steel, A. S. Bracker, D. Gammon, and L. Sham, Coherent population trapping of an electron spin in a single negatively charged quantum dot, Nat. Phys. **4**, 692 (2008).

[21] D. Press, T. D. Ladd, B. Zhang, and Y. Yamamoto, Complete quantum control of a single quantum dot spin using ultrafast optical pulses, Nature (London) **456**, 218 (2008).

[22] B. Pingault, J. N. Becker, C. H. Schulte, C. Arend, C. Hepp, T. Godde, A. I. Tartakovskii, M. Markham, C. Becher, and M. Atatüre, All-Optical Formation of Coherent Dark States of Silicon-Vacancy Spins in Diamond, Phys. Rev. Lett. **113**, 263601 (2014).

[23] L. J. Rogers, K. D. Jahnke, M. H. Metsch, A. Sipahigil, J. M. Binder, T. Teraji, H. Sumiya, J. Isoya, M. D. Lukin, and P. Hemmer, All-Optical Initialization, Readout, and Coherent Preparation of Single Silicon-Vacancy Spins in Diamond, Phys. Rev. Lett. **113**, 263602 (2014).

[24] J. Bochmann, M. Mücke, C. Guhl, S. Ritter, G. Rempe, and D. L. Moehring, Lossless State Detection of Single Neutral Atoms, Phys. Rev. Lett. **104**, 203601 (2010).

[25] R. Gehr, J. Volz, G. Dubois, T. Steinmetz, Y. Colombe, B. L. Lev, R. Long, J. Estève, and J. Reichel, Cavity-Based Single Atom Preparation and High-Fidelity Hyperfine State Readout, Phys. Rev. Lett. **104**, 203602 (2010).

[26] J. Volz, R. Gehr, G. Dubois, J. Estève, and J. Reichel, Measurement of the internal state of a single atom without energy exchange, Nature (London) **475**, 210 (2011).

[27] A. Young, C. Hu, L. Marseglia, J. Harrison, J. O'Brien, and J. Rarity, Cavity enhanced spin measurement of the ground state spin of an NV center in diamond, New J. Phys. **11**, 013007 (2009).

[28] S. A. Wolf, I. Rosenberg, R. Rapaport, and N. Bar-Gill, Purcell-enhanced optical spin readout of nitrogen-vacancy centers in diamond, Phys. Rev. B **92**, 235410 (2015).

[29] C. O'Brien, T. Zhong, A. Faraon, and C. Simon, Nondestructive photon detection using a single rare-earth ion coupled to a photonic cavity, Phys. Rev. A **94**, 043807 (2016).

[30] S. Sun and E. Waks, Single-shot optical readout of a quantum bit using cavity quantum electrodynamics, Phys. Rev. A **94**, 012307 (2016).

[31] S. Hughes and H. Kamada, Single-quantum-dot strong coupling in a semiconductor photonic crystal nanocavity side coupled to a waveguide, Phys. Rev. B **70**, 195313 (2004).

[32] E. Waks and J. Vuckovic, Dipole Induced Transparency in Drop-Filter Cavity-Waveguide Systems, Phys. Rev. Lett. **96**, 153601 (2006).

[33] J.-T. Shen and S. Fan, Theory of single-photon transport in a single-mode waveguide. I. Coupling to a cavity containing a two-level atom, Phys. Rev. A **79**, 023837 (2009).

[34] T. Belhadj, T. Amand, A. Kunold, C.-M. Simon, T. Kuroda, M. Abbarchi, T. Mano, K. Sakoda, S. Kunz, and X. Marie, Impact of heavy hole-light hole coupling on optical selection rules in GaAs quantum dots, Appl. Phys. Lett. **97**, 051111 (2010).

[35] See Supplemental Material at http://link.aps.org/supplemental/10.1103/PhysRevApplied.9.054013 for detailed theoretical analysis and supporting experimental results.

[36] Y. Arakawa, S. Iwamoto, M. Nomura, A. Tandaechanurat, and Y. Ota, Cavity quantum electrodynamics and lasing oscillation in single quantum dot-photonic crystal nanocavity coupled systems, IEEE J. Sel. Top. Quantum Electron. **18**, 1818 (2012).

[37] Y. Akahane, T. Asano, B.-S. Song, and S. Noda, Fine-tuned high-Q photonic-crystal nanocavity, Opt. Express **13**, 1202 (2005).

[38] P. Lodahl, S. Mahmoodian, and S. Stobbe, Interfacing single photons and single quantum dots with photonic nanostructures, Rev. Mod. Phys. **87**, 347 (2015).

[39] D. Englund, A. Faraon, I. Fushman, N. Stoltz, P. Petroff, and J. Vučković, Controlling cavity reflectivity with a single quantum dot, Nature (London) **450**, 857 (2007).

[40] M. Atatüre, J. Dreiser, A. Badolato, A. Högele, K. Karrai, and A. Imamoglu, Quantum-dot spin-state preparation with near-unity fidelity, Science **312**, 551 (2006).

[41] S. Sun, H. Kim, G. S. Solomon, and E. Waks, A quantum phase switch between a single solid-state spin and a photon, Nat. Nanotechnol. **11**, 539 (2016).

[42] D. Englund, D. Fattal, E. Waks, G. Solomon, B. Zhang, T. Nakaoka, Y. Arakawa, Y. Yamamoto, and J. Vučković, Controlling the Spontaneous Emission Rate of Single Quantum Dots in a Two-Dimensional Photonic Crystal, Phys. Rev. Lett. **95**, 013904 (2005).

[43] M. A. Nielsen and I. Chuang, *Quantum Computation and Quantum Information* (Cambridge University Press, New York, 2002).

[44] S. Combrié and A. De Rossi, Directive emission from high-Q photonic crystal cavities through band folding, Phys. Rev. B **79**, 041101(R) (2009).

[45] X. Ding, Y. He, Z.-C. Duan, N. Gregersen, M.-C. Chen, S. Unsleber, S. Maier, C. Schneider, M. Kamp, and S. Höfling, On-Demand Single Photons with High Extraction

Efficiency and Near-Unity Indistinguishability from a Resonantly Driven Quantum Dot in a Micropillar, Phys. Rev. Lett. **116**, 020401 (2016).

[46] N. Somaschi, V. Giesz, L. De Santis, J. Loredo, M. P. Almeida, G. Hornecker, S. L. Portalupi, T. Grange, C. Antón, and J. Demory, Near-optimal single-photon sources in the solid state, Nat. Photonics **10**, 340 (2016).

[47] T. Tiecke, K. Nayak, J. Thompson, T. Peyronel, N. De Leon, V. Vuletić, and M. Lukin, Efficient fiber-optical interface for nanophotonic devices, Optica **2**, 70 (2015).

[48] S. G. Carter, T. M. Sweeney, M. Kim, C. S. Kim, D. Solenov, S. E. Economou, T. L. Reinecke, L. Yang, A. S. Bracker, and D. Gammon, Quantum control of a spin qubit coupled to a photonic crystal cavity, Nat. Photonics **7**, 329 (2013).

[49] K. G. Lagoudakis, K. Fischer, T. Sarmiento, A. Majumdar, A. Rundquist, J. Lu, M. Bajcsy, and J. Vučković, Deterministically charged quantum dots in photonic crystal nanoresonators for efficient spin–photon interfaces, New J. Phys. **15**, 113056 (2013).

[50] R. Bose, D. Sridharan, G. Solomon, and E. Waks, Observation of strong coupling through transmission modification of a cavity-coupled photonic crystal waveguide, Opt. Express **19**, 5398 (2011).

[51] G. Reithmaier, S. Lichtmannecker, T. Reichert, P. Hasch, K. Müller, M. Bichler, R. Gross, and J. Finley, On-chip time resolved detection of quantum dot emission using integrated superconducting single photon detectors, Sci. Rep. **3**, 1901 (2013).

[52] G. Reithmaier, M. Kaniber, F. Flassig, S. Lichtmannecker, K. Müller, A. Andrejew, J. Vučković, R. Gross, and J. Finley, On-chip generation, routing, and detection of resonance fluorescence, Nano Lett. **15**, 5208 (2015).